Supporting Information

Decoding the infrared spectra changes upon formation of molecular complexes: The case of halogen bonding in pyridine···perfluorohaloarene complexes

Alex Iglesias-Reguant,[a,b] Heribert Reis,[c] Miroslav Medveď,[d,e] Borys Ośmiałowski,[a] Robert Zaleśny,*[,f] Josep M. Luis*[,b]

[a] *Faculty of Chemistry, Nicolaus Copernicus University, Gagarina 7, PL-87100 Toruń, Poland*

[b] *Institute of Computational Chemistry and Catalysis and Department of Chemistry, University of Girona, Campus de Montilivi, 17003, Girona, Catalonia, Spain*

[c] *Institute of Chemical Biology, National Hellenic Research Foundation (NHRF), Vassileos Constantinou Ave 48th, 116 35 Athens, Greece.*

[d] *Department of Chemistry, Faculty of Natural Sciences, Matej Bel University, Tajovského 40, SK-97400 Banská Bystrica, Slovak Republic.*

[e] *Regional Centre of Advanced Technologies and Materials, Czech Advanced Technology and Research Institute (CATRIN), Palacký University in Olomouc, Šlechtitelů 27, 783 71 Olomouc, Czech Republic*

[f] *Faculty of Chemistry, Wroclaw University of Science and Technology, Wybrzeże Wyspiańskiego 27, 50-370 Wrocław, Poland*

E-mail: josepm.luis@udg.edu (J.M.L.), robert.zalesny@pwr.edu.pl (R.Z.)

Software and computational details

Field-free equilibrium structures of **pyr**:C_6F_5X were obtained employing the MP2 method in combination with Dunning's correlation-consistent aug-cc-pVDZ basis set.[1] For the heavy atoms (bromine and iodine), the corresponding effective core potential (aug-cc-pVDZ-PP)[2] were applied to include scalar relativistic effects. Kozuch and Martin[3] showed that relativistic ECP in combination with the non-relativistic Hamiltonian provides binding energies of XB systems in excellent agreement with those obtained using the all-electron Douglas–Kroll (DK) Hamiltonian. Field-free equilibrium structures of HCN:BrF, HCN:IF, HCN:HCl, HCN:HNC, and HCN:HCN dimers were obtained at the MP2 level in combination with Dunning's correlation-consistent aug-cc-pVTZ basis set.[2] Harmonic vibrational analysis was performed at the same level of theory to confirm that the optimized structures were true minima. All field-free computations were performed with the Gaussian program.[4] Field-dependent geometry optimizations and property calculations were carried out using custom computer programs.[5] VP-EDS calculations were performed using a modified in-house version of the Gamess (US) program.[6] The VP-EDS partitioning of the excess properties is fully consistent with the utilization of the MP2 method for the evaluation of the total electronic and nuclear-relaxation properties of complexes. Our choice of the basis set was based on a study performed by some of[7] which showed that for medium-sized systems aug-cc-pVDZ provides reliable results for both electronic and nuclear-relaxation (hyper)polarizabilities. In the FF-NR approach,[5] it is necessary to apply an identical level of theory for both the field-dependent geometry optimization and property calculations. This requirement imposes certain constraints on the *ab initio* method and the size of the basis set that can be utilized. In a previous study[8] of our group we concluded that MP2 is a reliable method for the analysis of both electronic and vibrational properties of XB complexes and, in particular, for unraveling the interplay of interaction types contributing to the excess (hyper)polarizabilities.

All the harmonical vibrational calculations can be accessed at `http://dx.doi.org/10.19061/iochem-bd-4-62` onto the IOCHEM-BD platform (`www.iochem-bd.org`) to facilitate data exchange and dissemination, according to the FAIR principles of OpenData sharing.

Table S1: Intermolecular interaction energy decomposition for **pyr**:C_6F_5X complexes, where X is Cl, Br, or I, performed at the MP2/aug-cc-pVDZ(PP) level of theory. All values are given in kcal/mol.

	$\varepsilon_{el}^{(10)}$	ΔE_{ex}^{HL}	ΔE_{del}^{HF}	$\varepsilon_{el,r}^{(12)}$	$\varepsilon_{disp}^{(20)}$	$\Delta E_{ex}^{(2)}$	ΔE_{int}^{HF}	ΔE_{corr}^{MP2}	ΔE_{int}^{MP2}
pyr:C_6F_5Cl	-5.183	7.163	-1.579	-0.549	-4.786	1.860	0.401	-3.475	-3.074
pyr:C_6F_5Br	-11.000	14.810	-4.171	-1.141	-6.804	3.235	-0.361	-4.711	-5.072
pyr:C_6F_5I	-19.310	26.082	-8.798	-1.803	-9.299	5.381	-2.027	-5.722	-7.749

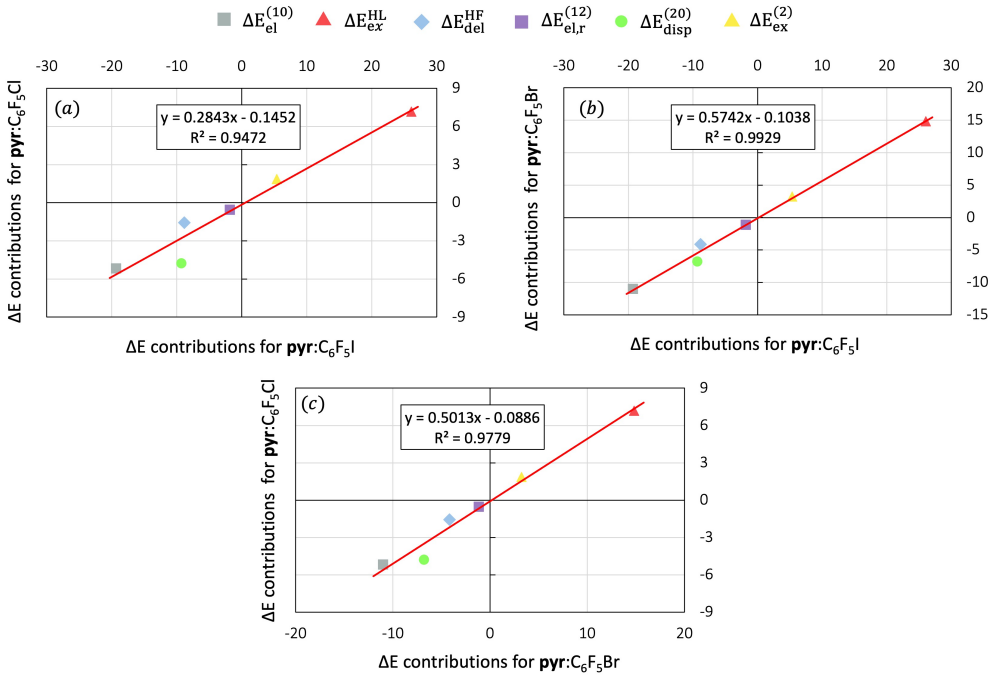

Figure S1: Linear correlation between partition terms of the interaction energy of (a) **pyr**:C_6F_5I and **pyr**:C_6F_5Br, (b) **pyr**:C_6F_5I and **pyr**:C_6F_5Cl and (c) the **pyr**:C_6F_5Br and **pyr**:C_6F_5Cl complexes. Energies are given in kcal/mol.

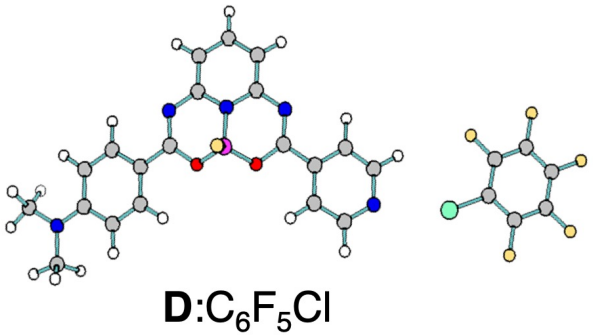

D:C_6F_5Cl

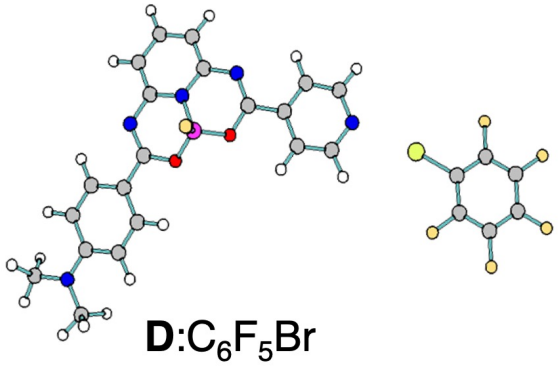

D:C_6F_5Br

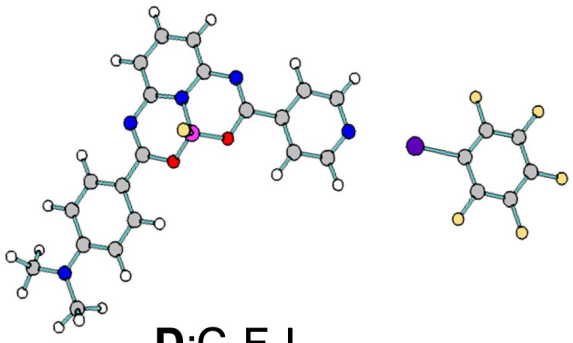

D:C_6F_5I

Figure S2: Ground state equilibrium geometries of **D**:C_6F_5X complexes optimized at MN15/aug-cc-pVDZ(PP) level of theory obtained from ref. [9]

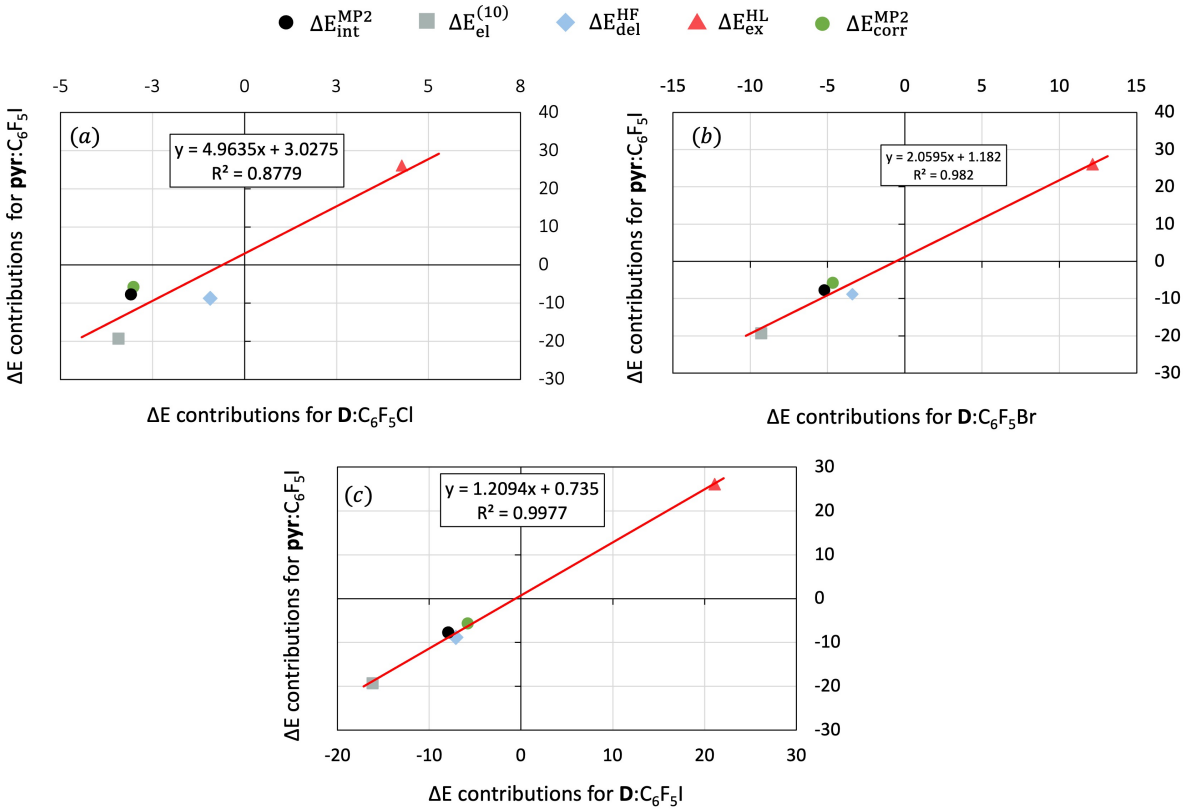

Figure S3: Linear correlation between partition terms of the interaction energy of **pyr**:C_6F_5I and (a) **D**:C_6F_5Cl, (b) **D**:C_6F_5Br and (c) **D**:C_6F_5I complexes. Energies are given in kcal/mol.

Table S2: Intermolecular interaction energy partitioning of **D**:C_6F_5X complexes at RI-MP2/aug-cc-pVDZ(PP) level of theory. All values are given in kcal/mol.

	$\varepsilon_{el}^{(10)}$	ΔE_{ex}^{HL}	ΔE_{del}^{HF}	ΔE_{int}^{HF}	ΔE_{corr}^{RI-MP2}	ΔE_{int}^{RI-MP2}
D:C_6F_5Cl	-3.421	4.279	-0.927	-0.069	-3.017	-3.086
D:C_6F_5Br	-9.288	12.136	-3.393	-0.545	-4.652	-5.197
D:C_6F_5I	-16.140	21.091	-7.083	-2.132	-5.794	-7.926

Table S3: Coefficient of determination (R^2) of the linear fits between partition terms of the intermolecular interaction energy of all halogen-bonded and hydrogen-bonded complexes studied in this work and π-π stacking (benzene:trifluorobenzene, trifluorobenzene:trifluorobenzene, and hexafluorobenzene:trifluorobenzene) systems studied in ref. 17.

	pyr:C6F5Cl	pyr:C6F5Br	pyr:C6F5I	HCN-IF	HCN-BrF	HCN-HCl	HCN-HNC	HCN-HCN	ben-tri	tri-tri
pyr:C6F5Br	0.97									
pyr:C6F5I	0.93	0.99								
HCN-IF	0.89	0.96	0.99							
HCN-BrF	0.90	0.97	0.99	1.00						
HCN-HCl	0.92	0.97	0.98	0.98	0.98					
HCN-HNC	0.81	0.88	0.91	0.91	0.89	0.96				
HCN-HCN	0.74	0.81	0.83	0.82	0.80	0.90	0.97			
ben-tri	0.88	0.78	0.71	0.65	0.69	0.67	0.50	0.43		
tri-tri	0.86	0.76	0.68	0.63	0.66	0.64	0.46	0.39	1.00	
hex-tri	0.88	0.78	0.70	0.65	0.68	0.66	0.49	0.41	1.00	1.00

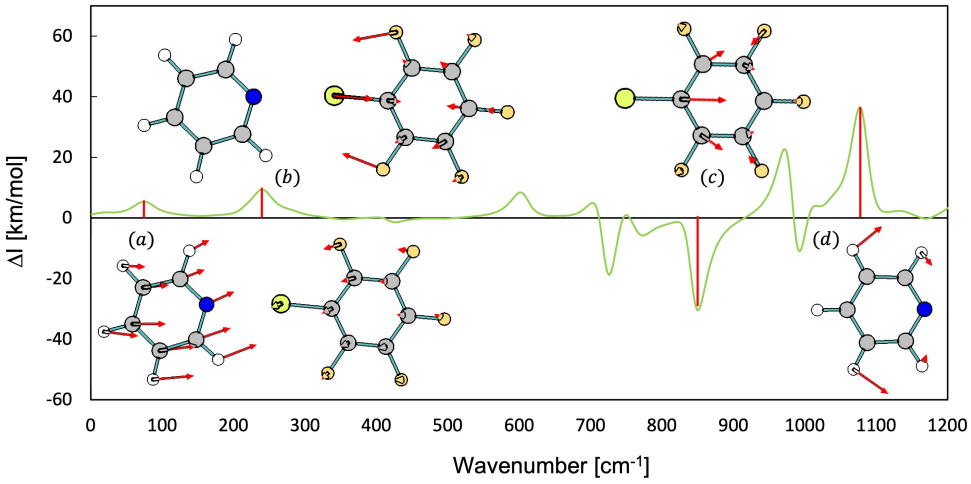

Figure S4: Difference IR spectrum obtained by subtracting the simulated IR spectra of **pyr** and C_6F_5Br from the IR spectrum of the **pyr**:C_6F_5Br complex, as well as the displacements of: a) an intermolecular vibrational stretching mode (ν_a^{int}), b) C-X stretching of C_6F_5Br, which involves a change in the halogen bond distance (ν_b^{C-X}), c) one local vibrational mode from C_6F_5Br that involves the distortion of the aromatic cycle ($\nu_c^{C_6F_5Br}$) , and d) a rocking in-plane bending of the hydrogens of the pyridine (ν_c^{pyr}).

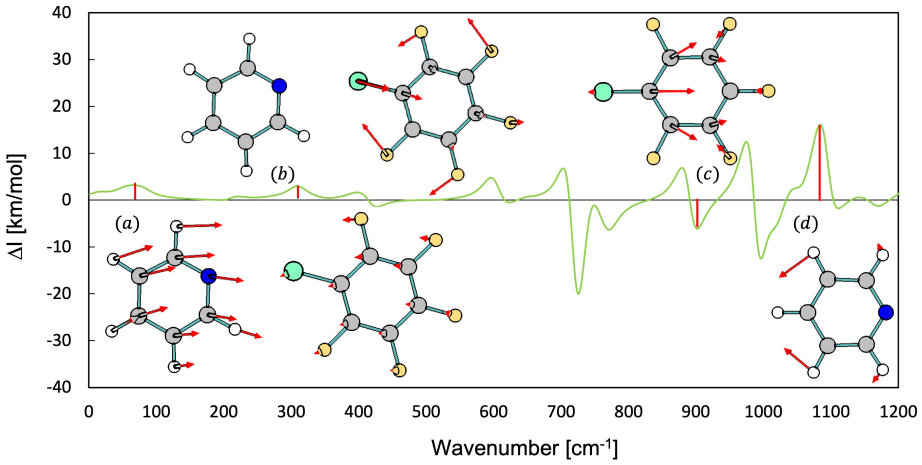

Figure S5: Difference IR spectrum obtained by subtracting the simulated IR spectra of **pyr** and C_6F_5Cl from the IR spectrum of **pyr**:C_6F_5Cl complex and the displacements of: a) an intermolecular vibrational stretching mode (ν_a^{int}), b) C-X stretching of C_6F_5Cl, which involves a change in the halogen bond distance (ν_b^{C-X}), c) one local vibrational mode from C_6F_5Br that involves the distortion of the aromatic cycle ($\nu_c^{C_6F_5Cl}$), and d) a rocking in-plane bending of the hydrogens of the pyridine (ν_c^{pyr}).

Table S4: Coefficient of determination (R^2) of the linear fits between partition terms of the interaction energy of **pyr**:C_6F_5X and the shift in frequency upon complexation for ν_a^{int}, ν_b^{C-X}, $\nu_c^{C_6F_5X}$, and ν_d^{pyr} vibrational modes

vibrational mode	$\Delta E_{el}^{(10)}$	ΔE_{ex}^{HL}	ΔE_{del}^{HF}	$\Delta E_{el,r}^{(12)}$	$\Delta E_{disp}^{(20)}$	$\Delta E_{ex}^{(2)}$
ν_a^{int}	0.97	0.96	0.94	0.99	0.98	0.96
ν_b^{C-X}	1.00	1.00	1.00	1.00	1.00	1.00
$\nu_c^{C_6F_5X}$	0.96	0.96	0.94	0.99	0.98	0.95
ν_d^{pyr}	0.38	0.39	0.44	0.31	0.34	0.40

Table S5: Excess IR intensity partitioning of the four studied vibrational modes for the **pyr**:C_6F_5Cl complex at MP2/aug-cc-pVDZ(PP) level of theory. All values are given in km/mol.

vibrational mode	$\Delta I_{el}^{(10)}$	ΔI_{ex}^{HL}	ΔI_{del}^{HF}	$\Delta I_{el,r}^{(12)}$	$\Delta I_{disp}^{(20)}$	$\Delta I_{ex}^{(2)}$	ΔI_{int}^{HF}	ΔI_{corr}^{MP2}	ΔI_{int}^{MP2}
ν_a^{int}	3.89	-5.79	1.92	0.56	1.11	-0.91	0.02	0.76	0.78
ν_b^{C-X}	4.22	-3.04	1.92	0.31	0.73	-0.31	3.11	0.77	3.88
$\nu_c^{C_6F_5Cl}$	14.86	-8.16	-6.70	1.46	2.62	-6.41	1.17	-3.21	-2.04
ν_d^{pyr}	4.32	-3.88	2.16	1.29	0.43	-0.43	2.59	0.43	3.02

Table S6: Excess IR intensity partitioning of the studied vibrational modes for the **pyr**:C_6F_5Br complex at MP2/aug-cc-pVDZ(PP) level of theory. All values are given in km/mol.

vibrational mode	$\Delta I_{el}^{(10)}$	ΔI_{ex}^{HL}	ΔI_{del}^{HF}	$\Delta I_{el,r}^{(12)}$	$\Delta I_{disp}^{(20)}$	$\Delta I_{ex}^{(2)}$	ΔI_{int}^{HF}	ΔI_{corr}^{MP2}	ΔI_{int}^{MP2}
ν_a^{int}	8.09	-13.49	5.96	0.98	2.27	-1.55	0.70	1.70	2.40
ν_b^{C-X}	18.34	-19.01	13.65	1.16	4.23	-1.08	12.87	4.31	17.18
$\nu_c^{C_6F_5Br}$	10.13	-17.66	-12.98	4.41	3.89	-10.65	-20.51	-3.21	-23.63
ν_d^{pyr}	4.75	0.00	1.73	1.73	0.00	-0.43	6.48	-0.43	6.04

Table S7: Excess IR intensity partitioning of the studied vibrational modes for the **pyr**:C_6F_5I complex at MP2/aug-cc-pVDZ(PP) level of theory. All values are given in km/mol.

vibrational mode	$\Delta I_{el}^{(10)}$	ΔI_{ex}^{HL}	ΔI_{del}^{HF}	$\Delta I_{el,r}^{(12)}$	$\Delta I_{disp}^{(20)}$	$\Delta I_{ex}^{(2)}$	ΔI_{int}^{HF}	ΔI_{corr}^{MP2}	ΔI_{int}^{MP2}
ν_a^{int}	33.83	-53.92	28.59	3.06	5.04	-6.42	8.50	1.68	10.18
ν_b^{C-X}	36.93	-34.93	32.23	1.44	6.26	-2.87	34.24	4.97	39.21
$\nu_c^{C_6F_5I}$	5.51	13.66	-55.37	6.23	5.27	-9.35	-32.84	2.16	-30.92
ν_d^{pyr}	13.81	25.88	-23.73	4.31	0.86	-2.59	15.96	2.59	18.54

Table S8: Coefficient of determination (R^2) of the linear fits between the excess IR intensity and the interaction energy for the four studied vibrational modes of **pyr**:C_6F_5X complexes (second column); and between the excess IR intensity contributions and interaction energy contributions for each vibrational mode for each molecular complex.

Vibrational mode	ΔE vs ΔI^i	**pyr**:C_6F_5Cl	**pyr**:C_6F_5Br	**pyr**:C_6F_5I
ν_a^{int}	0.93	0.89	0.93	0.93
ν_b^{C-X}	1.00	0.78	0.89	0.88
$\nu_c^{C_6F_5X}$	0.88	0.57	0.62	0.08
ν_d^{pyr}	0.94	0.76	0.41	0.22

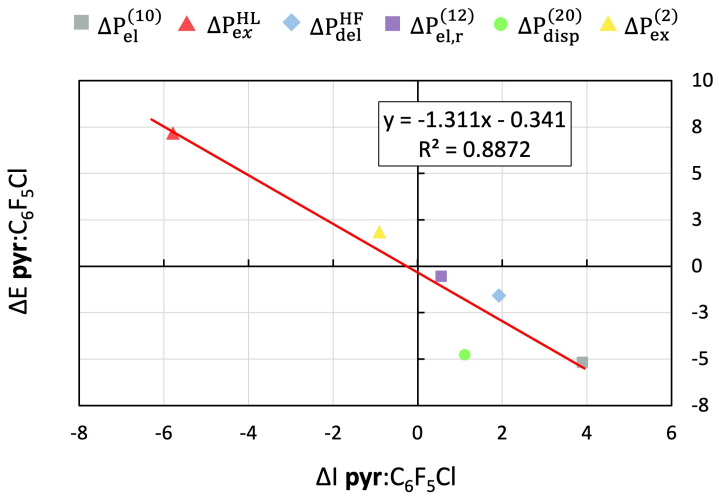

Figure S6: Linear fits between interaction-type contributions for the interaction energy ($\Delta P = \Delta E$) and the corresponding terms of the excess IR intensity ($\Delta P = \Delta I$) for ν_a^{int} for the **pyr**:C_6F_5Cl complex. Energies are given in kcal/mol and intensities in km/mol.

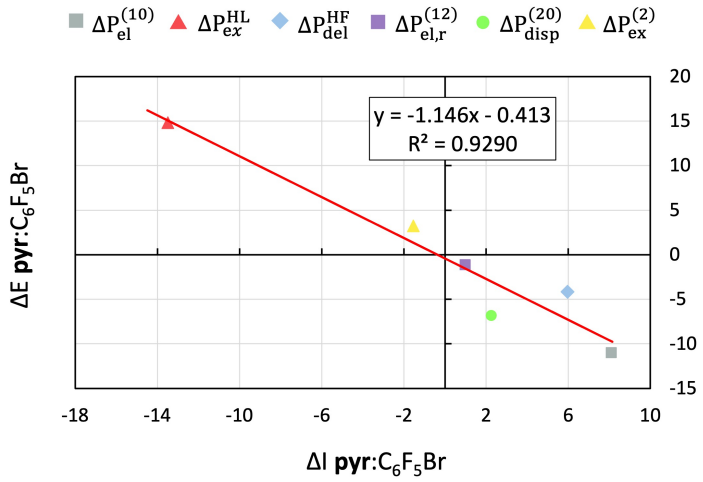

Figure S7: Linear fits between interaction-type contributions for the interaction energy ($\Delta P = \Delta E$) and the corresponding terms of the excess IR intensity ($\Delta P = \Delta I$) for ν_a^{int} for the **pyr**:C_6F_5Br complex. Energies are given in kcal/mol and intensities in km/mol.

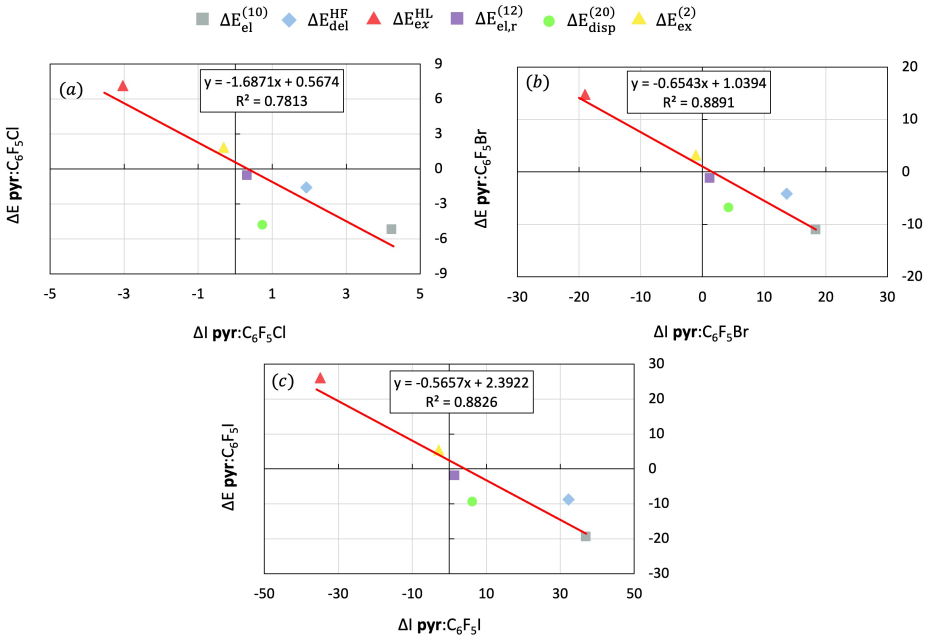

Figure S8: Linear fit between the partition terms for the interaction energy and the corresponding terms of the excess IR intensity for ν_b^{C-X} for (a) **pyr**:C_6F_5Cl, (b) **pyr**:C_6F_5Br and (c) **pyr**:C_6F_5I complexes. Energies are given in kcal/mol and intensities in km/mol.

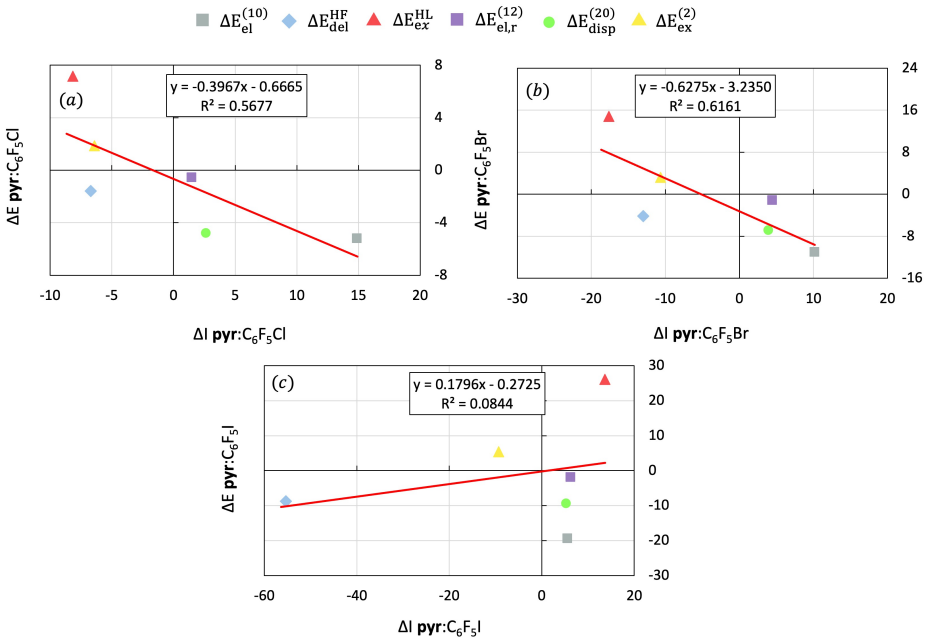

Figure S9: Linear fit between the partition terms for the interaction energy and the corresponding terms of the excess IR intensity for $\nu_c^{C_6F_5X}$ for the (a) **pyr**:C_6F_5Cl, (b) **pyr**:C_6F_5Br and (c) **pyr**:C_6F_5I complexes. Energies are given in kcal/mol and intensities in km/mol.

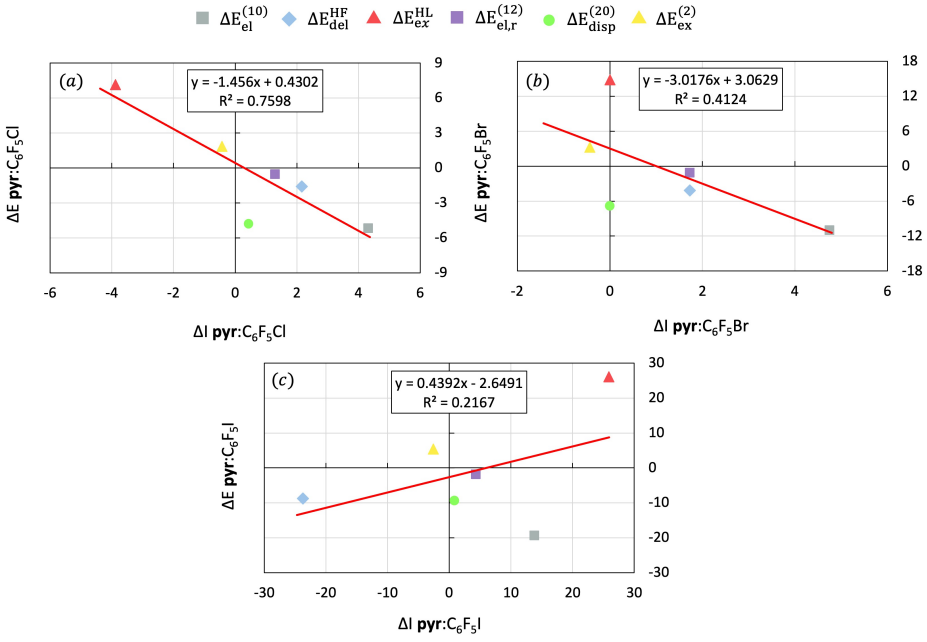

Figure S10: Linear fit between the partition terms for the interaction energy and the corresponding terms of the excess IR intensity for ν_d^{pyr} for the (a) **pyr**:C_6F_5Cl, (b) **pyr**:C_6F_5Br and (c) **pyr**:C_6F_5I complexes. Energies are given in kcal/mol and intensities in km/mol.

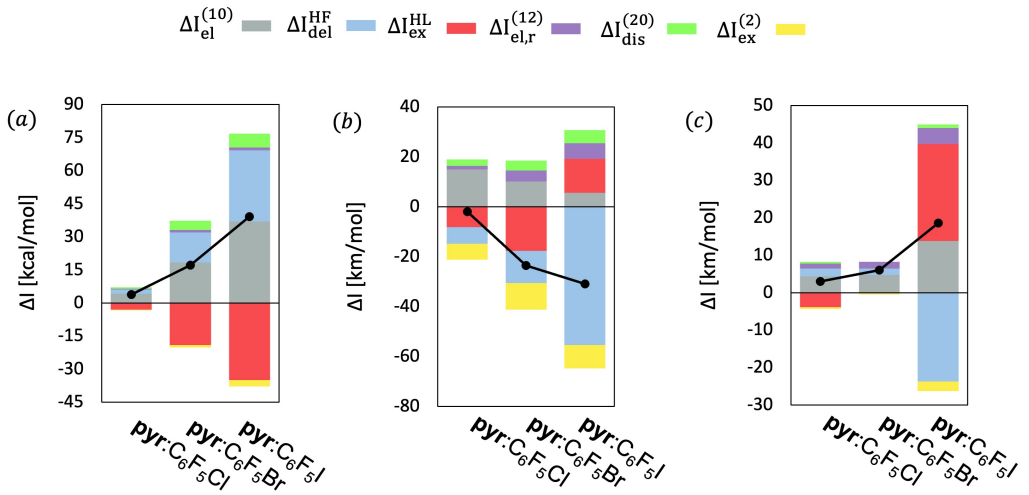

Figure S11: Excess IR intensity partitioning of the a) ν_b^{C-X}, b) $\nu_c^{C_6F_5X}$ and c) ν_d^{pyr} for the **pyr**:C_6F_5X complexes at the equilibrium geometries at MP2/aug-cc-pVDZ-PP level of theory.

Table S9: Intermolecular interaction energy decomposition for a series of small complexes performed at the MP2/aug-cc-pVTZ(PP) level of theory. All values are given in kcal/mol.

	$\varepsilon_{el}^{(10)}$	ΔE_{ex}^{HL}	ΔE_{del}^{HF}	$\varepsilon_{el,r}^{(12)}$	$\varepsilon_{disp}^{(20)}$	$\Delta E_{ex}^{(2)}$	ΔE_{int}^{HF}	ΔE_{corr}^{MP2}	ΔE_{int}^{MP2}
HCN:IF	-23.610	34.649	-15.484	-1.248	-10.438	6.109	-4.445	-5.576	-10.021
HCN:BrF	-19.969	30.441	-12.830	-1.064	-9.577	4.798	-2.358	-5.843	-8.201
HCN:HCl	-8.439	10.210	-3.824	-0.087	-3.980	1.284	-2.053	-2.783	-4.836
HCN:HNC	-10.222	9.368	-4.186	-0.518	-3.405	1.411	-5.040	-2.512	-7.552
HCN:HCN	-6.9200	4.978	-1.893	0.362	-2.198	1.029	-3.835	-0.806	-4.641

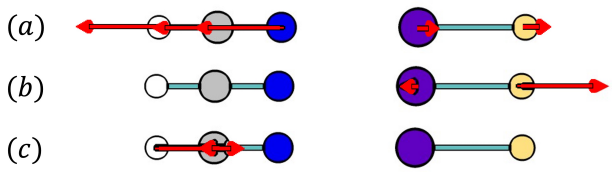

Figure S12: Displacements of a) an intermolecular vibrational stretching mode, b) I-F stretching and c) H-C stretching located on the HCN monomer for the HCN:IF dimer.

Table S10: Excess IR intensity partitioning of the studied vibrational modes for the HCN:IF complex at MP2/aug-cc-pVTZ(PP) level of theory. All values are given in km/mol.

vibrational mode	$\Delta I_{el}^{(10)}$	ΔI_{ex}^{HL}	ΔI_{del}^{HF}	$\Delta I_{el,r}^{(12)}$	$\Delta I_{disp}^{(20)}$	$\Delta I_{ex}^{(2)}$	ΔI_{int}^{HF}	ΔI_{corr}^{MP2}	ΔI_{int}^{MP2}
Intermolecular	28.72	-39.37	32.79	-0.51	-3.66	-2.45	22.14	-6.64	15.50
I-F stretching	49.96	19.25	71.72	-11.34	-2.64	5.54	139.74	-8.44	130.78
H-C stretching	65.85	-17.56	35.12	4.39	0.00	4.39	83.41	8.78	92.19

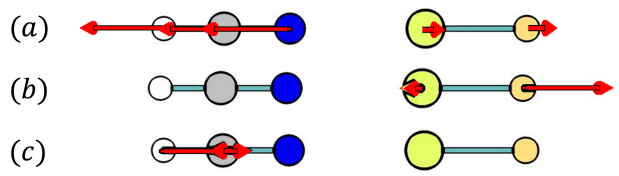

Figure S13: Displacements of a) an intermolecular vibrational stretching mode, b) Br-F stretching and c) H-C stretching located on the HCN monomer for the HCN:BrF dimer.

Table S11: Excess IR intensity partitioning of the studied vibrational modes for the HCN:BrF complex at MP2/aug-cc-pVTZ(PP) level of theory. All values are given in km/mol.

vibrational mode	$\Delta I_{\mathrm{el}}^{(10)}$	$\Delta I_{\mathrm{ex}}^{\mathrm{HL}}$	$\Delta I_{\mathrm{del}}^{\mathrm{HF}}$	$\Delta I_{\mathrm{el,r}}^{(12)}$	$\Delta I_{\mathrm{disp}}^{(20)}$	$\Delta I_{\mathrm{ex}}^{(2)}$	$\Delta I_{\mathrm{int}}^{\mathrm{HF}}$	$\Delta I_{\mathrm{corr}}^{\mathrm{MP2}}$	$\Delta I_{\mathrm{int}}^{\mathrm{MP2}}$
Intermolecular	63.43	-118.83	71.19	2.88	8.84	-11.09	16.62	0.20	16.82
Br-F stretching	62.08	0.77	96.04	-11.52	2.00	-1.23	159.04	-10.91	148.13
H-C stretching	57.23	-17.61	26.41	0.00	0.00	4.40	66.04	4.40	70.44

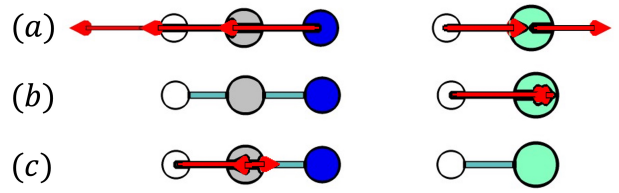

Figure S14: Displacements of a) an intermolecular vibrational stretching mode, b) H-Cl stretching and c) H-C stretching located on the HCN monomer for the HCN:HCl dimer.

Table S12: Excess IR intensity partitioning of the studied vibrational modes for the HCN:HCl complex at MP2/aug-cc-pVTZ(PP) level of theory. All values are given in km/mol.

vibrational mode	$\Delta I_{\mathrm{el}}^{(10)}$	$\Delta I_{\mathrm{ex}}^{\mathrm{HL}}$	$\Delta I_{\mathrm{del}}^{\mathrm{HF}}$	$\Delta I_{\mathrm{el,r}}^{(12)}$	$\Delta I_{\mathrm{disp}}^{(20)}$	$\Delta I_{\mathrm{ex}}^{(2)}$	$\Delta I_{\mathrm{int}}^{\mathrm{HF}}$	$\Delta I_{\mathrm{corr}}^{\mathrm{MP2}}$	$\Delta I_{\mathrm{int}}^{\mathrm{MP2}}$
Intermolecular	10.42	-18.17	12.96	-0.05	2.27	-1.37	5.21	0.86	6.06
H-Cl stretching	799.63	-503.58	961.38	-33.57	152.60	18.31	1257.42	134.29	1391.72
H-C stretching	26.54	-8.85	4.42	4.42	0.00	0.00	22.12	4.42	26.54

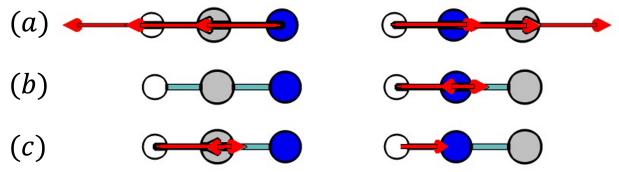

Figure S15: Displacements of a) an intermolecular vibrational stretching mode, b) H-N stretching and c) H-C stretching located on the HCN monomer for the HCN:HNC dimer.

Table S13: Excess IR intensity partitioning of the studied vibrational modes for the HCN:HNC complex at MP2/aug-cc-pVTZ(PP) level of theory. All values are given in km/mol.

vibrational mode	$\Delta I_{el}^{(10)}$	ΔI_{ex}^{HL}	ΔI_{del}^{HF}	$\Delta I_{el,r}^{(12)}$	$\Delta I_{disp}^{(20)}$	$\Delta I_{ex}^{(2)}$	ΔI_{int}^{HF}	ΔI_{corr}^{MP2}	ΔI_{int}^{MP2}
Intermolecular	7.43	-10.58	8.85	-0.33	0.50	-0.33	5.70	-0.17	5.54
H-N stretching	935.14	-305.45	1024.42	-108.08	65.79	126.88	1696.41	84.59	1766.90
H-C stretching	61.35	-8.76	30.68	4.38	0.00	4.38	83.27	8.76	92.03

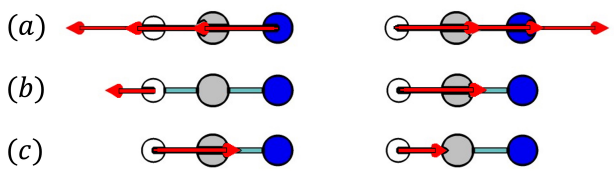

Figure S16: Displacements of a) an intermolecular vibrational stretching mode, b) H-C stretching located on the right-hand HCN monomer and c) H-C stretching located on the left-hand side HCN monomer for the HCN:HCN dimer.

Table S14: Excess IR intensity partitioning of the studied vibrational modes for the HCN:HCN complex at MP2/aug-cc-pVTZ(PP) level of theory. All values are given in km/mol.

vibrational mode	$\Delta I_{el}^{(10)}$	ΔI_{ex}^{HL}	ΔI_{del}^{HF}	$\Delta I_{el,r}^{(12)}$	$\Delta I_{disp}^{(20)}$	$\Delta I_{ex}^{(2)}$	ΔI_{int}^{HF}	ΔI_{corr}^{MP2}	ΔI_{int}^{MP2}
Intermolecular	4.92	-6.61	3.51	-0.14	0.96	-0.71	1.83	0.10	1.93
H-C (A)	144.85	-21.95	122.90	-8.78	8.78	17.56	241.41	13.17	254.58
H-C (B)	175.57	-39.50	105.34	-4.39	13.17	241.41	8.78	17.58	254.58

Table S15: Coefficient of determination (R^2) for the linear regression between the excess IR intensity contributions and interaction energy contributions for three vibrational modes of small X:B and H:B complexes.

complex	stretching			intermolecular
	H-R	X-F	H-C	
HCN:IF	-	0.20	0.67	0.86
HCN:BrF	-	0.34	0.65	0.94
HCN:HCl	0.73	-	0.67	0.87
HCN:HNC	0.64	-	0.71	0.83
HCN:HCN	0.65	-	0.80	0.88

References

[1] K. A. Peterson, D. Figgen, E. Goll, H. Stoll and M. Dolg, *J. Chem. Phys.*, 2003, **119**, 11113–11123.

[2] K. A. Peterson, B. C. Shepler, D. Figgen and H. Stoll, *J. Phys. Chem. A*, 2006, **110**, 13877–13883.

[3] S. Kozuch and J. M. L. Martin, *J. Chem. Theory Comput.*, 2013, **9**, 1918–1931.

[4] M. J. Frisch, G. W. Trucks, H. B. Schlegel, G. E. Scuseria, M. A. Robb, J. R. Cheeseman, G. Scalmani, V. Barone, G. A. Petersson, H. Nakatsuji, X. Li, M. Caricato, A. V. Marenich, J. Bloino, B. G. Janesko, R. Gomperts, B. Mennucci, H. P. Hratchian, J. V. Ortiz, A. F. Izmaylov, J. L. Sonnenberg, D. Williams-Young, F. Ding, F. Lipparini, F. Egidi, J. Goings, B. Peng, A. Petrone, T. Henderson, D. Ranasinghe, V. G. Zakrzewski, J. Gao, N. Rega, G. Zheng, W. Liang, M. Hada, M. Ehara, K. Toyota, R. Fukuda, J. Hasegawa, M. Ishida, T. Nakajima, Y. Honda, O. Kitao, H. Nakai, T. Vreven, K. Throssell, J. A. Montgomery, Jr., J. E. Peralta, F. Ogliaro, M. J. Bearpark, J. J. Heyd, E. N. Brothers, K. N. Kudin, V. N. Staroverov, T. A. Keith, R. Kobayashi, J. Normand, K. Raghavachari, A. P. Rendell, J. C. Burant, S. S. Iyengar, J. Tomasi, M. Cossi, J. M. Millam, M. Klene, C. Adamo, R. Cammi, J. W. Ochterski, R. L. Martin, K. Morokuma, O. Farkas, J. B. Foresman and D. J. Fox, *Gaussian~16 Revision C.01*, 2016, Gaussian Inc. Wallingford CT.

[5] J. M. Luis, M. Duran, J. L. Andrés, B. Champagne and B. Kirtman, *J. Chem. Phys.*, 1999, **111**, 875.

[6] M. W. Schmidt, K. K. Baldridge, J. A. Boatz, S. T. Elbert, M. S. Gordon, J. H. Jensen, S. Koseki, N. Matsunaga, K. A. Nguyen, S. Su, T. L. Windus, M. Dupuis and J. A. Montgomery Jr, *J. Comput. Chem.*, 1993, **14**, 1347–1363.

[7] R. Zaleśny, A. Baranowska-Łączkowska, M. Medveď and J. M. Luis, *J. Chem. Theory Comput.*, 2015, **11**, 4119–4128.

[8] M. Medved', A. Iglesias-Reguant, H. Reis, R. W. Góra, J. M. Luis and R. Zaleśny, *Phys. Chem. Chem. Phys.*, 2020, **22**, 4225–4234.

[9] A. Iglesias-Reguant, J. Zielak-Milewska, T. Misiaszek, R. Zaleśny, J. M. Luis and B. Ośmiałowski, *J. Org. Chem.*, 2022, **87**, 15159–15165.